RSC Advances

PAPER

View Article Online
View Journal | View Issue

Cite this: *RSC Adv.*, 2026, **16**, 19702

Research on the mechanism of P and F in phosphogypsum stabilized by humic acid synergized with group metallic triad-based curing agent

Kezhen Chen,†[ab] Jiangtao Shang,†[b] Yingying Cai,*[cd] Qiong Hu,[b] Heng Li[e] and Xiong Tong*[a]

The high levels of soluble phosphorus (P) and fluorine (F) in phosphogypsum (PG) pose a significant environmental challenge to the sustainable development of the P chemical industry. In this research, we present a green and low-cost stabilization strategy that employs a synergistic combination of organic and inorganic additives to effectively suppress the release of P and F from PG. Through batch experiments, we systematically evaluated the effects of humic acid (HA) synergized with inorganic curing agents on the leaching behavior of contaminants, with a focus on their impact on pH and immobilization efficiency of P and F. The optimal formulation consisted of 5 wt% type-II humic acid (HA-2) combined with 1 wt% type-II group-synergistic metallic triad-based curing agent (GMT-2). Under simulated leaching conditions representative of surface and groundwater exposure, this material yielded a leachate with a pH of 5.51, P concentration of 0.1 mg L^{-1}, and F concentration of 0.9 mg L^{-1}, which complies with China's class III surface water quality standards (GB 3838-2002). The underlying stabilization mechanisms of the combined system leverage physical coating, chemical precipitation, and a distinctive bridged ternary complexation mechanism to construct a denser and more stable immobilization layer on the PG surface, in which the integrated approach achieves a durable synergistic fixation of P and F. This work provides a practical method for the environmentally sound management and sustainable utilization of PG.

Received 13th February 2026
Accepted 28th March 2026

DOI: 10.1039/d6ra01271j

rsc.li/rsc-advances

1 Introduction

Phosphogypsum (PG), a byproduct of phosphoric acid production, consists primarily of calcium sulfate dihydrate ($CaSO_4 \cdot 2H_2O$) but contains various impurities, including phosphates, fluorides, heavy metals, residual acids, naturally occurring radionuclides, and rare earth elements.[1] The large-scale stockpiling of PG poses significant environmental challenges, occupying vast land areas and creating persistent ecological risks. Heavy metals and radionuclides in PG can bioaccumulate, causing toxicity to flora, fauna, and ultimately human health.[2] A critical concern is the generation of leachate, which is rich in soluble phosphate (P) and fluoride (F), during storage. Typical PG contains 0.1–1.5% of F and 0.1–2.0% of P_2O_5, with the leachable concentrations of PO_4^{3-} and F^- frequently exceeding the Chinese national standard limits (GB 8978-1996).[3] This leachate can directly contaminate surface and groundwater, leading to eutrophication and potential risks to aquatic life and human health.[4] The P ions are linked to dermatitis, soil contamination, and water quality deterioration,[5] while F bioaccumulation through the food chain can disrupt nutrient metabolism and affect teeth, cardiac tissue, and skeletal muscles.[6] Consequently, developing effective strategies to mitigate the environmental impact of PG is imperative.

Common PG treatment technologies include solidification/stabilization (S/S),[7] washing,[8] acid/alkali treatment,[9] flotation,[10] thermal processing,[11] and biotechnological methods.[12] Among these, the S/S has garnered widespread attention due to its operational simplicity, relatively low cost, and proven efficacy in reducing the leaching of contaminants. Conventional S/S employs inorganic cementitious materials like cement and lime. These materials hydrate upon mixing with PG, forming gels, such as calcium silicate hydrate (C–S–H) and calcium

[a]*Faculty of Land and Resources Engineering, Kunming University of Science and Technology, Kunming, Yunnan, 650093, China. E-mail: kgxiongtong@163.com*
[b]*Yunnan Academy of Ecological and Environmental Sciences, Co., Ltd, Kunming, Yunnan, 650032, China*
[c]*Faculty of Environmental Science and Engineering, Kunming University of Science and Technology, Kunming, Yunnan, 650500, China. E-mail: caiyymail@kust.edu.cn*
[d]*National-Regional Engineering Center for Recovery of Waste Gases from Metallurgical and Chemical Industries, Kunming, Yunnan, 650500, China*
[e]*Yunnan Yuntianhua Environmental Protection Technology Co., Ltd, Kunming, Yunnan, 650228, China*
† These authors contributed equally to this work.

aluminate hydrate (C–A–H), that fill pores and encapsulate particles, thereby physically restricting the release of harmful substances.[13] Chemically, the lime treatment precipitates PO_4^{3-} and F^- as less soluble $Ca_3(PO_4)_2$ and CaF_2, though its cost remains a constraint.[14] Recent advancements include using the PG-steel slag blends to densify the carbonation matrix, enhancing the Pb^{2+} and Cr^{3+} immobilization by 80% and 87%, respectively,[15] as well as employing reactive stabilizers that form insoluble precipitates or complexes.[16,17] For instance, the addition of 0.2–0.5 wt% biochar was shown to effectively reduce the leaching of F from PG backfill materials.[18]

The current PG utilization routes encompass building materials (*e.g.*, plaster, boards, blocks),[19,20] soil remediation, chemical production, wastewater treatment,[21] and mine backfilling.[22–24] However, global utilization rates of PG remain low. With an annual production of nearly 300 million tons, approximately 58% is stockpiled, 28% is discharged into marine systems, and only 14% is recycled. Major barriers for a widespread reuse include the high cost and difficulty of impurity removal, low economic viability of products, and persistent concerns about secondary pollution from the PG-derived materials. Therefore, exploring green and economically feasible detoxification methods is essential for enhancing PG recycling.

Humic acid (HA), a natural organic polymer, has emerged as a promising amendment for environmental remediation. Its high surface area, porous structure, and abundance of active functional groups (*e.g.*, carboxyl, hydroxyl, and phenolic –OH) enable complexation/chelation with metal ions and interactions with anions like phosphate and fluoride.[25] These interactions can lead to the formation of stable complexes or insoluble compounds, reducing the mobility of contaminants. For example, HA–Al^{3+} chelates have been used to adsorb F and mitigate its accumulation in tea plants.[26] Concurrently, the

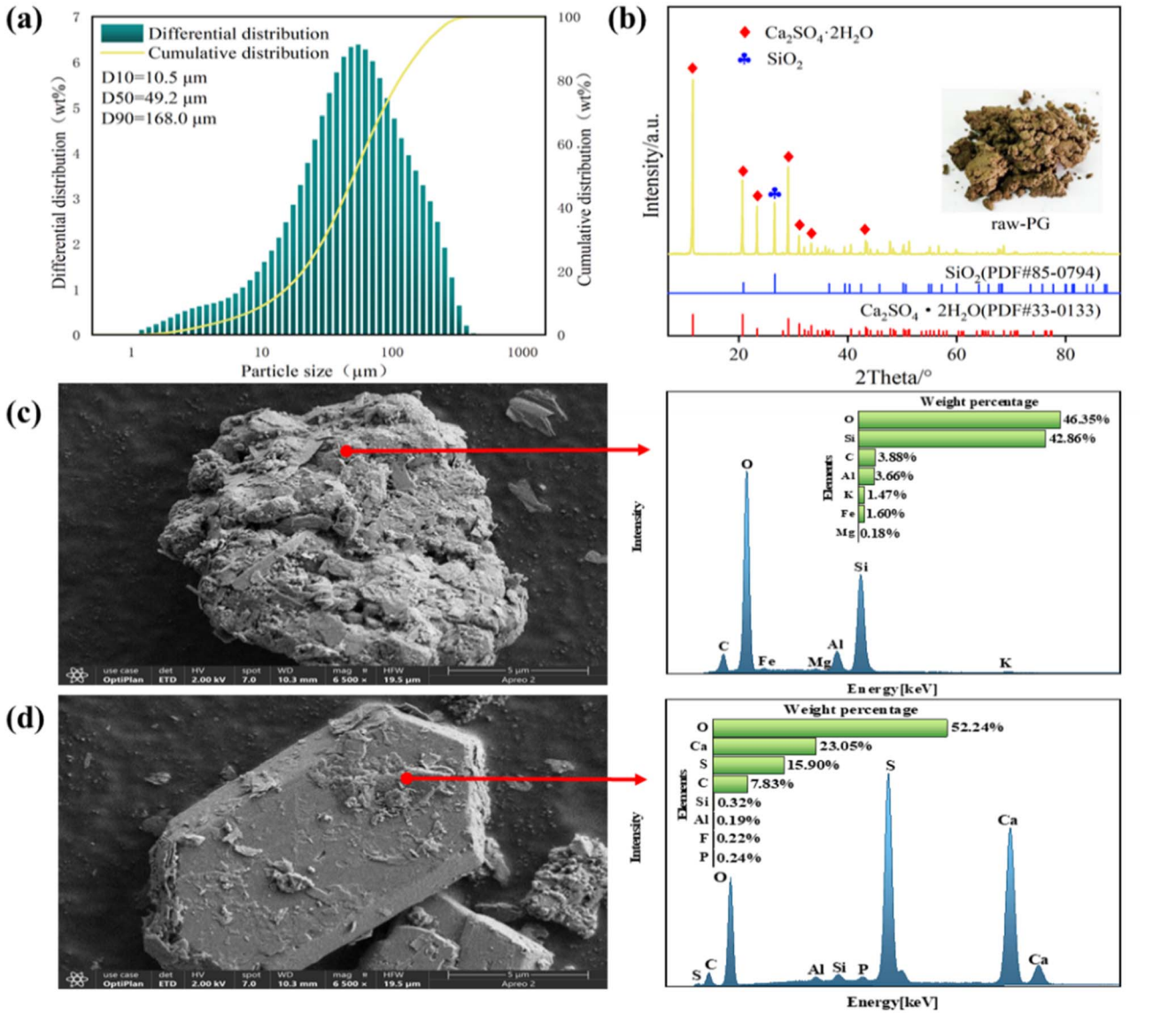

Fig. 1 Physicochemical properties of PG: (a) particle size, (b) XRD analysis, and (c) and (d) SEM and matching EDX data analysis at different points.

potential of metal-based compounds for anion immobilization is well-established.[27] P and F anions, owing to their high electronegativity, can form stable precipitates with cations such as Ca^{2+}, $Fe^{2+/3+}$ and Mg^{2+}.[28] Materials like mesoporous metal oxides (MgO, Al_2O_3) show promise as phosphate adsorbents,[29] and engineered calcium silicate hydrates have achieved 95% P and 50% F removal.[30] Notably, mechanochemically synthesized Ca/Al/La layered double hydroxides exhibit superior performance in controlling water-soluble phosphorus from PG.[31] Despite these advances in the immobilization of P and F anions, a significant research gap exists regarding the synergistic use of organic additives like HA and tailored inorganic metal-based curing agents for the concurrent immobilization of P and F from PG. Most existing S/S approaches focus on single-contaminant systems or lack a mechanistic understanding of the stabilization process under conditions that simulate natural leaching.

Building upon the S/S, a synergistic treatment strategy employing HA in combination with a group-synergistic metallic triad-based curing agent (GMT) is proposed in this study. The core objective is to achieve an effective and concurrent immobilization of P and F, thereby detoxifying PG for potential safe utilization. To unravel the underlying stabilization mechanisms, a multifaceted analytical approach was employed, including X-ray diffraction (XRD), scanning electron microscopy (SEM), Fourier-transform infrared spectroscopy (FT-IR), X-ray photoelectron spectroscopy (XPS), and Brunauer–Emmett–Teller (BET) surface area analysis. The research aims to furnish both a theoretical foundation and practical technical support for enabling the large-scale, environmentally benign utilization of PG.

2 Materials and methods

2.1 Samples and chemical reagents

The PG sample was sourced from Yunnan Tianbao Animal Nutrition Technology Co., Ltd, China. As shown in Fig. 1(a), the material exhibits a brown color, particle size distribution ranging from 0 to 200 μm, D_{50} of 49.2 μm and D_{90} of 168 μm. Its moisture content was measured as 19.76%. The XRD analysis (Fig. 1(b)) identified gypsum dihydrate (70.4%) and quartz (39.6%) as the primary crystalline phases. SEM imaging (Fig. 1(c)) revealed a heterogeneous microstructure composed of irregular plate-like gypsum crystals intergrown with other impurity phases, displaying rough surfaces and distinct layered aggregations. Energy-dispersive spectroscopy (EDS) analysis confirmed the presence of P and F within the sample. Bulk chemical composition analysis indicates that the PG is predominantly composed of CaO, SO_3, and SiO_2, which together account for 76.35% of its mass (Table 1). The contents of P_2O_5 and F were determined to be 1.3% and 0.2%, respectively.

Table 1 Elemental analysis results of PG

Component	SiO_2	Al_2O_3	CaO	SO_3	Fe_2O_3	P_2O_5
Content (%)	22.46	1.09	21.88	32.01	0.51	1.30
Component	F	MgO	Na_2O	K_2O	TiO_2	Other
Content (%)	0.20	0.36	0.66	0.38	0.12	18.83

As shown in Table S1, various elements were detected in the leaching solution of PG. The leaching concentrations of F and total P were 23.3 mg L^{-1} and 47.7 mg L^{-1} respectively. According to the Chinese 'Surface Water Environmental Quality Standards, the leaching concentrations of F and P in surface water class III exceeded the standards by 23.3 and 238.5 times, respectively. In addition, the pH of PG was 3.62, which was lower than the pH range (6–9) stipulated in the surface water class III standard.

The HA was purchased from the Sigma Aldrich (CAS:1415-93-6). And the GMT was purchased from Beijing Runming Environmental Technology Co., LTD. From the XRD analysis of HA (Fig. 2(a)), it can be seen that the composition is relatively complex, and there may be multiple associated or impurity components. According to Table 2, the main elements of HA are O, Ca, S, Al, and Fe. The content of other elements not detected in HA-2 is higher than that in HA-3, mainly consisting of carbon-containing organic matter. The main elements of GMT are Ca, Cl, Al, Mg, Si, and Fe. The XRD analysis of GMT (Fig. 2(b)) shows that GMT exhibits amorphous characteristics. The diffraction peaks of GMT-2 are relatively wide and diffuse, while the peaks of GMT-1 are relatively sharp, indicating that the crystalline structure of GMT-1 is more ordered than that of GMT-2.

2.2 Sample preparation and characterization

2.2.1 Sample preparation and experiment design scheme. The preparation of solidified samples followed these key steps: (1) removal of large impurities from the raw PG, followed by sieving through a 100-mesh sieve (2) thorough homogenization of PG with curing agents according to the designed formulations; (3) addition of an appropriate amount of water to facilitate sufficient reactions among the constituents; (4) curing of mixtures for a fixed period of 7 days. The treated samples were subsequently evaluated for changes in leachate pH, P and F leaching concentrations, and their chemical speciation.

The experimental investigation proceeded in two stages. First, the effects of HA (0, 2.5, 5, 7.5, 10, and 12.5 wt%) and GMT (0, 0.5, 1, 1.5, 2, and 2.5 wt%) on the mobility of soluble P and F impurities were examined, respectively. This initial screening identified the most effective types of HA and GMT. Subsequently, the optimized materials (designated HA-2 and GMT-2) were selected for composite stabilization treatments to study the influence of organic–inorganic (HA-GMT) synergy on the pH and contaminant release behavior of the solidified PG. A follow-up orthogonal test matrix was designed, involving HA-2 additions of 2.5, 5, 7.5, 10, 12.5, and 15 wt% combined with the GMT-2 additions of 0.5, 1, 2, and 3 wt%, to determine their optimal combination ratio. The systematic optimization of curing parameters of the composite provides critical data to support the environmentally sound utilization of PG.

2.2.2 P and F extraction experiments and index determination. The leaching risk of contaminants from PG under simulated surface water exposure was assessed in accordance

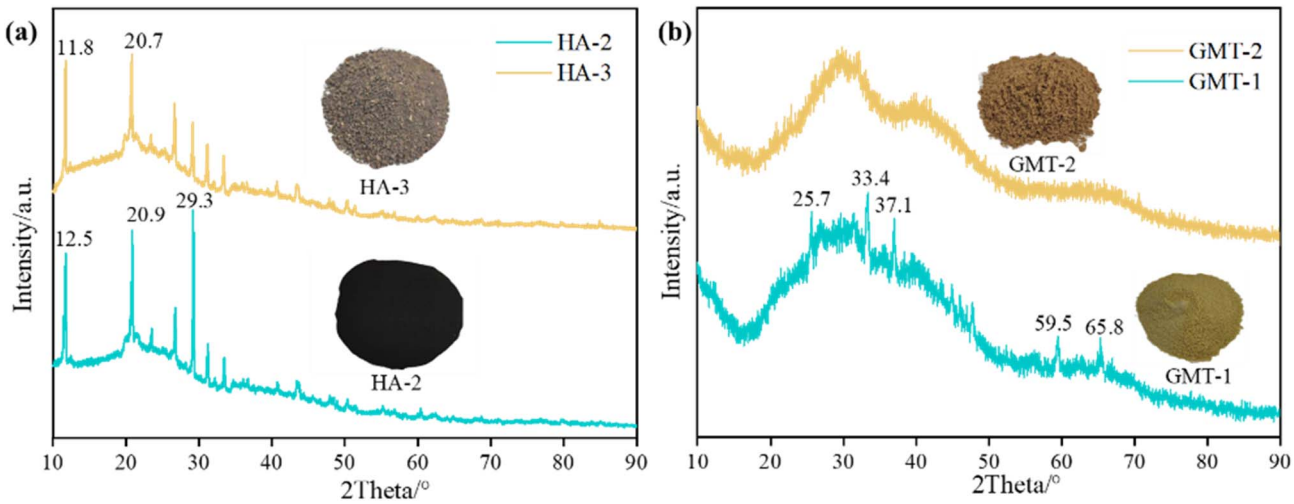

Fig. 2 XRD patterns of different types of (a) HA and (b) GMT solidified materials.

Table 2 Chemical compositions of different types of HA and GMT (wt%)

Component (%)	O	Ca	Cl	Al	Si	Mg	Fe	S	Na	K
GMT-1	—	38.2	32.3	11.1	5.5	0.54	7.38	1.01	—	0.71
GMT-2	—	38.8	40.1	11.8	3.45	0.44	3.25	0.96	0.3	0.74
HA-2	20.0	5.1	—	1.7	2.1	0.6	7.3	4.1	0.06	0.2
HA-3	33.7	3.6	—	6.1	11.0	0.7	7.9	7.4	—	0.5

with the Chinese standard Solid Waste—Extraction Procedure for Leaching Toxicity—Horizontal Vibration Method (HJ 557-2010). The PG sample was first dried at 105 °C to determine its moisture content. Deionized water was then added at a liquid-to-solid ratio of 10 : 1 (L kg^{-1}). The mixture was subjected to horizontal vibration at room temperature with a frequency of (110 ± 10) oscillations per minute and an amplitude of 40 mm for 8 hours, followed by a 16 hour settling period. The resulting leachate was filtered through a 0.45 μm membrane filter for subsequent analysis. The concentrations of total P and F in the filtered leachate were determined using the ammonium molybdate spectrophotometric method (GB 11893-89) with a UV-Vis spectrophotometer (model TOC-L), and the F ion-selective electrode method (GB 7484-87) with a fluoride electrode (model PF-2-01), respectively. The sequential P extraction procedure was performed according to the standards, as outlined in Fig. S1(a). This method fractionates P into five operationally defined forms as total phosphorus (TP), inorganic phosphorus (IP), organic phosphorus (OP), non-apatite inorganic phosphorus (NAIP), and apatite inorganic phosphorus (AP). The sequential extraction procedure fractionated F into five operationally defined species as the water-soluble fraction (Ws-F), exchangeable fraction (Ex-F), Fe/Mn oxide-bound fraction (Fe/Mn-F), organically-bound fraction (Or-F), and residual fraction (Res-F), as shown in Fig. S1(b). The pH value was measured potentiometrically at a water-to-soil ratio of 2.5 : 1 using a pH electrode (model PHSJ-6L).

2.2.3 Analysis and characterization. Particle size distribution was determined by laser diffraction analysis (BT-9300H, Bettersize Instruments Ltd, Dandong, China). Solid samples were dried at 45 ± 5 °C prior to mineralogical characterization using XRD (D8 ADVANCE, Bruker, Germany). Morphological features were examined by field-emission scanning electron microscopy (FE-SEM, SU5000, Hitachi, Japan). The functional groups of the samples were analyzed by FTIR (Nicolet Nexus 670, Thermo Fisher Scientific, USA) over a wavenumber range of 4000–400 cm^{-1}. Surface elemental composition and chemical states were investigated using XPS (Escalab 250Xi, Thermo Fisher Scientific, USA). Specific surface area and pore size distribution were obtained from nitrogen adsorption–desorption isotherms measured with a surface area and porosity analyzer (ASAP 2020 Plus 2.00, Micromeritics, USA).

3 Results and discussion

3.1 Effect of HA and GMT on the release of harmful substances

3.1.1 The change in pH. The effects of different types and mass ratios of HA and GMT on the pH of PG are shown in Fig. 3. The pH of PG gradually increased with the addition of HA or GMT. Moreover, at equivalent mass ratios, the GMT exerted a greater influence on the system pH than HA, attributable to its higher content of alkaline components such as calcium.[32] Fig. 3(a) illustrates the variation in pH with the addition of

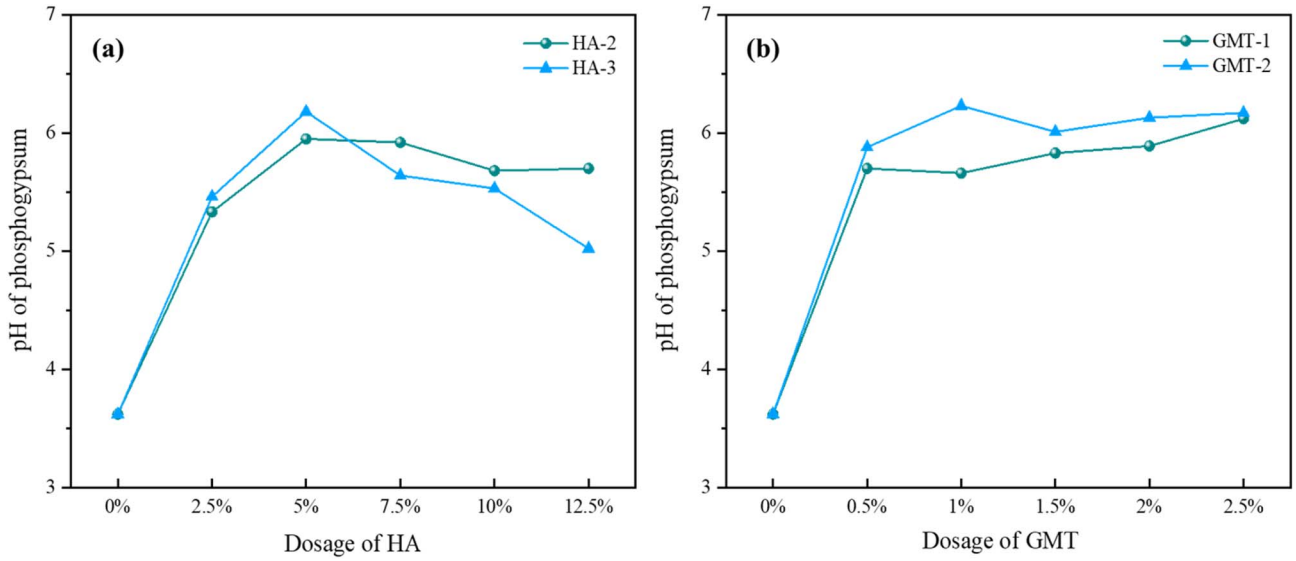

Fig. 3 Effect of the addition of different types of HA and GMT on the pH (reaction time is 1 d) (a) HA and (b) GMT.

different HAs. Both HA types elevated the pH at low mass ratios. When the mass ratio was below 5%, the pH rose rapidly with the increasing addition amount. From 2.5% to 5%, the pH increased more gradually. For HA-2, it increased from 5.33 to 5.92, and for HA-3, from 5.46 to 6.18. However, when the mass ratio exceeded 5%, the pH began to decline. The pH of both the HA solutions exhibited a turning point with concentration. In the low-concentration range (≤5%), the slight pH increase can be attributed to the weak alkalization resulting from carboxyl dissociation.[33] At higher concentrations, the hydrophobic micellar aggregates shielded the ionizable active sites, thereby reducing their pH-modulating capacity. Notably, HA-3 showed a more pronounced pH drop above 5% addition, with the pH at 12.5% being lower than that at 2.5%. This is likely due to the higher aromatic condensation degree of HA-3, which promotes molecular stacking and enhances its hydrophobic nature.[34]

As shown in Fig. 3(b), the pH generally increased with a higher GMT mass ratio. GMT-1 showed a slight decrease at 1% addition, and GMT-2 at 1.5%, possibly due to localized agglomeration reducing the specific surface area or related to the two-stage kinetics of alkaline release.[35] At the same mass ratio, GMT-2 yielded a higher pH than GMT-1, likely because of its higher content of metallic components such as Ca, Mg, and Fe, which release more alkaline substances. The increase in pH is positively correlated with the CaO content in the raw materials, as metal ions together with sulfate (SO_4^{2-}) from PG activate slag reactions, continuously releasing OH^-. A higher pH environment also facilitates the stabilization of water-soluble P and F. It should be noted that, since no additional water was introduced, the inorganic curing agents could only utilize the attached and bound water in PG for hydration, which, to some extent, limited the increase in pH. This observation aligns with the mechanism reported by Chen *et al.*[36] From a practical standpoint, while HA organic materials offer advantages such as functional group diversity and P activation potential, their cost is relatively high. In contrast, GMT, as a conventional curing material, is widely used in engineering applications and is more cost-effective, though its pH response is significantly influenced by material composition and hydration conditions.

3.1.2 Release of P and F. We investigated the effects of the organic material HA and the inorganic material GMT on the leaching behavior of P and F from PG. The results are presented in Fig. 4(a). The addition of HA-2 significantly reduced the leaching concentrations of both P and F. At the HA-2 mass ratios of 2.5% and 5%, the P leaching concentrations were 7.22 mg L^{-1} and 1.83 mg L^{-1}, respectively, while the F leaching concentrations were 3.97 mg L^{-1} and 1.3 mg L^{-1}, respectively. Further increasing the HA-2 mass ratio did not enhance the immobilization of P and F, indicating that its adsorption sites were approaching saturation. Notably, HA-3 also reduced the leaching concentrations of P and F at a 5% mass ratio. However, when the mass ratio of HA-3 was increased from 5% to 12.5%, the leaching concentration of F showed an upward trend. These results indicate that while the HA-3 effectively immobilizes P, its efficiency in stabilizing F decreases after the mass ratio exceeds 2.5%. This decline may be attributed to an excessive amount of HA, which increases the capillary water content within the modified PG backfill material, thereby reducing the internal structural density and subsequently diminishing the adsorption efficiency.[37] In summary, the immobilization performance of HA-2 was superior to that of HA-3.

The evolution of the system pH shows a significant negative correlation with the release behavior of P and F. With the increasing addition of HA and GMT, the system pH rises rapidly from the initial low value and peaks at 5% HA or 1% GMT addition, during which the release concentrations of P and F in the leachate sharply decline, corresponding to a rapid increase in the solidification efficiency to over 90%. When the addition exceeds the aforementioned threshold, the pH in the HA group shows a slow decline, and the release concentrations of P and F

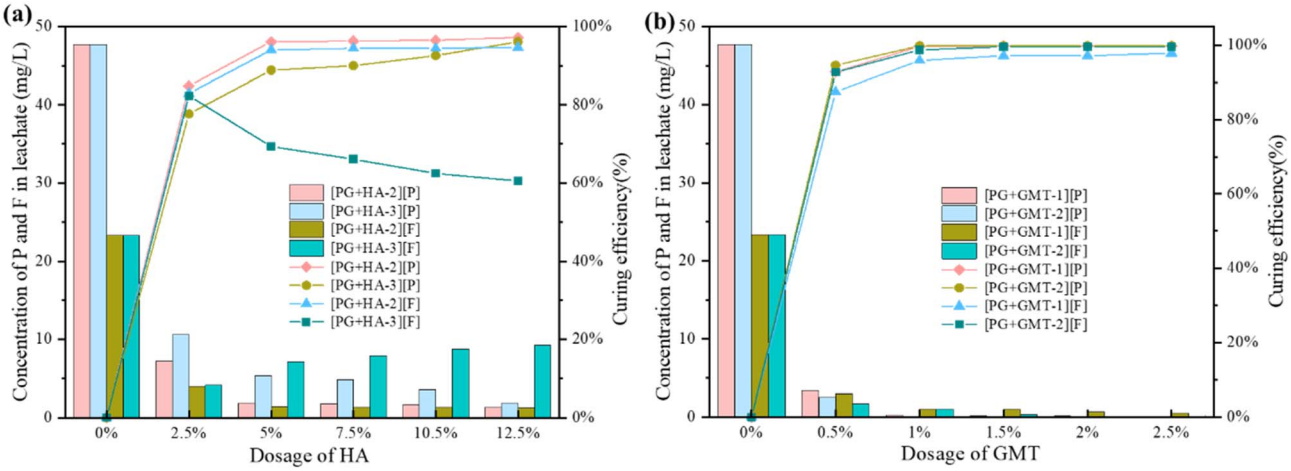

Fig. 4 Effect of the addition amount of HA and GMT on the leaching of P and F. Variation of the leaching concentration of P and F and curing efficiency with the addition of (a) HA and (b) GMT.

rise slightly, with a slight decrease in the solidification efficiency of F. In contrast, the pH in the GMT group remains at a high level with small fluctuations, and the release concentrations of P and F consistently stay at a very low level, with solidification efficiency stabilizing close to 100%. This result indicates that the construction of an alkaline environment is a core factor in suppressing the leaching of P and F. Higher pH values significantly reduce their mobility by promoting the formation of insoluble precipitates. Moreover, GMT, compared to HA, can maintain a stable high pH environment over a wider range of additions, thus demonstrating a more lasting and stable solidification effect on P and F.

As shown in Fig. 4(b), the GMT materials demonstrated a stronger synergistic immobilization capacity. Remarkably, GMT-2 achieved immobilization rates of 99.8% for P and 95.7% for F at a mere 1% mass ratio, outperforming GMT-1. This improved performance can be ascribed to its stronger ion-exchange and chemical precipitation capabilities. The study also verified that an alkaline environment is conducive to the stabilization of P and F, which is in line with the mechanism by which GMT enhances the effectiveness of immobilization.[38]

3.2 Effect of HA-2 synergized with GMT-2 on the release of harmful substances

3.2.1 The change of pH. The pH variation in HA-2 synergized with the GMT-2 composite system is shown in Fig. 5(a). The system exhibited good buffering capacity within the pH range of 5.05–6.23. As the mass ratio of HA-2 increased, the pH generally displayed a downward trend. However, when the mass ratio GMT-2 was 2.5%, a transient rise to 6.23 occurred after the HA-2 mass ratio reached 5%, followed by a subsequent decrease. Increasing the mass ratio of GMT-2 generally elevated the pH. Compared with single-component systems, the pH of the composite system is governed by the combined effect of the two additives. When the GMT-2 mass ratio exceeded 2%, it partially counteracted the acidifying effect of HA-2. Nevertheless, when the HA-2 mass ratio exceeded 12.5%, the pH of all the composite systems fell below the lowest value observed under single-factor conditions, indicating that high concentrations of HA-2 markedly suppress the alkalizing capability of GMT-2 through metal chelation and surface passivation, demonstrating a reversal effect.

3.2.2 Release of P and F. As shown in Fig. 5(b) and (c), the HA-2 synergized with the GMT-2 composite system exhibited

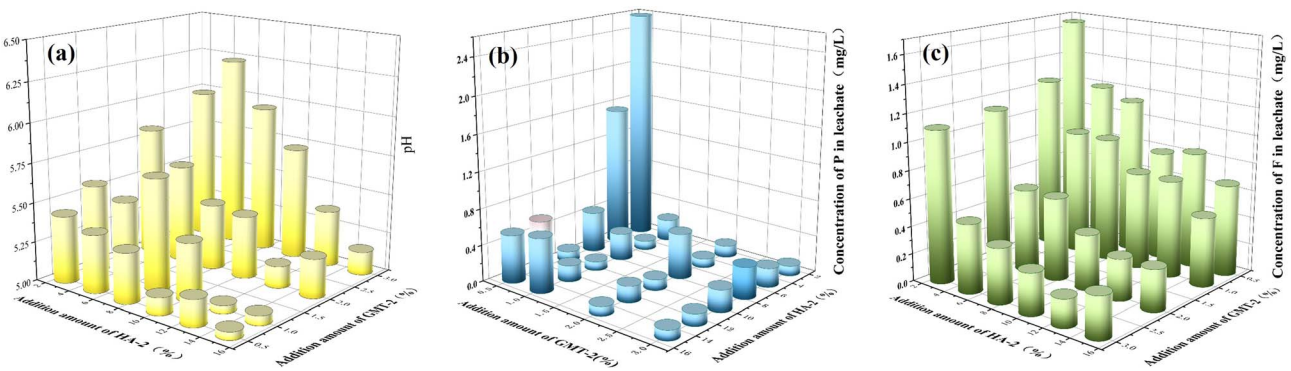

Fig. 5 Effect of the addition amount of HA-2-GMT-2 on (a) pH and the release of (b) P and (c) F.

a notable synergistic immobilization effect. When the HA mass ratio was fixed and the GMT mass ratio was gradually increased from 0.5% to 3%, the F concentration decreased continuously from 0.79 mg L^{-1} to 0.3 mg L^{-1}, while the P concentration remained consistently at an ultra-low level between 0.1 and 0.24 mg L^{-1}. It was notable that effective defluorination at high HA contents required higher GMT mass ratios correspondingly. In the system with 12.5% HA, increasing the GMT mass ratio from 0.5% to 3% reduced the F concentration from 0.84 mg L^{-1} to 0.2 mg L^{-1}, which represented a 76.2% decrease. In contrast, a low-HA and low-GMT combination (*e.g.*, 2.5% HA + 0.5% GMT) still resulted in residual concentrations of 2.58 mg L^{-1} for P and 1.66 mg L^{-1} for F, confirming that the composite system requires an optimized ratio to activate the synergistic immobilization effect.

In practical applications, besides the immobilization performance, economic viability constitutes a critical practical consideration. At a mass ratio of 5% HA-2 and 1% GMT-2, the solidification effect on PG was already highly significant, while the material cost remained relatively low. Further increasing the mass ratios of both components yielded only marginal improvements in the removal of soluble P and F. Therefore, based on an overall benefit assessment, a mass ratio of PG : HA-2 : GMT-2 = 94 : 5 : 1 was recommended. Under this condition, the leachate contained P at 0.1 mg L^{-1} and F at 0.9 mg L^{-1}, satisfying the class III water quality standards specified in the Environmental Quality Standards for Surface Water (GB 3838-2002).

System pH is a key factor in regulating the release of P and F. The pH peak triggered by GMT is higher, and the high pH range is wider. The corresponding low points of the F and P release concentrations are more significant and sustained, indicating that the P and F solidification effects achieved by GMT through pH regulation are superior to those of HA. The release concentration of F is more sensitive to pH changes, while the recovery amplitude of the P release concentration during the pH drop stage is relatively gentle, reflecting that the solidification stability of P in the system is slightly better than that of F.

3.2.3 Variation in the speciation of P and F. To elucidate the speciation distribution and immobilization mechanisms of P and F in PG, sequential extraction analyses were conducted on four samples (Fig. 6). Analysis of F speciation revealed that the total F content in all the treated groups was lower than that in the raw PG, indicating an effective reduction of soluble F. The overall distribution of F fractions followed the order as Res-F > Fe/Mn-F > Or-F > Ws-F > Ex-F. The Res-F was the dominant and the most stable fraction, exhibiting a low migration potential. Treatment with HA-2 led to a decrease in Or-F, likely due to the competitive complexation of metal ions by humic acid, which promoted the release of organically bound F.[39] The reduction in Or-F observed in the GMT-2 treated group can be attributed to the preferential precipitation of fluorine with metal ions such as Ca, Mg, and Fe.[40,41] The Ws-F showed a slight decrease after treatment, suggesting the adsorption and fixation of soluble F by both HA-2 and GMT-2, while Ex-F remained largely unchanged across the groups.

Analysis of P speciation showed that the content of NAIP was very low in all the samples, indicating the decomposition of apatite during phosphoric acid production. Upon the addition of HA-2, GMT-2, or their composite, the highly mobile OP fraction decreased, while the non-apatite IP fraction increased correspondingly. The total P content also decreased slightly. These findings suggest that the immobilization process facilitated the formation of stable, low-solubility P compounds, thereby reducing the leaching risk of P.[42,43]

3.3 Characterization

3.3.1 XRD and BET analyses. The XRD patterns of the raw PG sample and the three treated samples are presented in Fig. 7(a). The primary diffraction peaks in all the samples correspond to $CaSO_4 \cdot 2H_2O$ and SiO_2, confirming that the PG matrix consists predominantly of well-crystallized gypsum. After treatment with HA-2, GMT-2, or their composite, no new crystalline phases were detected. This indicates that the added components likely exist in a highly dispersed state, form solid solutions, or manifest as surface coatings.[44,45] Notably, the sample treated with the HA-2 and GMT-2 composite exhibited a marked reduction in diffraction peak intensities, particularly for $CaSO_4 \cdot 2H_2O$ and SiO_2, accompanied by varying degrees of peak broadening. This phenomenon is attributable to the combined action of HA-2 and GMT-2, suggesting that the immobilization treatment decreased the overall crystallinity of PG and increased its amorphous content. The attenuation in peak intensity can be attributed to three interrelated factors. First, the introduction of amorphous GMT-2 significantly increased the proportion of the amorphous phase within the system. Second, the surface reaction products of GMT-2 cementitious phases, such as ettringite ($3CaO \cdot Al_2O_3 \cdot 3CaSO_4 \cdot 32H_2O$) and anorthite ($CaAl_2Si_2O_8$), further promoted interparticle flocculation and coagulation. This enhanced aggregation contributes to the immobilization of P and F and is reflected in the XRD patterns by distinct peak shifts and intensity changes.[46,47]

The increased presence of these gel-forming phases is also a primary reason for the flocculation observed after the addition of GMT-2 and their predominant adsorption onto the surface of PG crystals.[20] Second, the macromolecular structure of HA-2 prevents its penetration into the inner layers of PG, leading primarily to the formation of a coating layer on the particle surfaces.[48,49] Third, metal ions such as Ca^{2+} and Mg^{2+} released predominantly by GMT-2 (and to a lesser extent by HA-2) react to form microcrystalline precipitates like $Ca_3(PO_4)_2$ and CaF_2, as well as cementitious products such as ettringite ($3CaO \cdot Al_2O_3 \cdot 3CaSO_4 \cdot 32H_2O$). These newly formed substances create an additional coating layer on the PG surface. Together, these layers collectively attenuate the diffraction signals. These processes not only reduce the relative content of the crystalline PG phase but also enhance the immobilization of P and F through surface modification and cementitious binding.

As shown in Fig. 7(b), the N_2 adsorption–desorption isotherms of PG samples treated with different types of HA and GMT additives all conform to type IV, accompanied by distinct

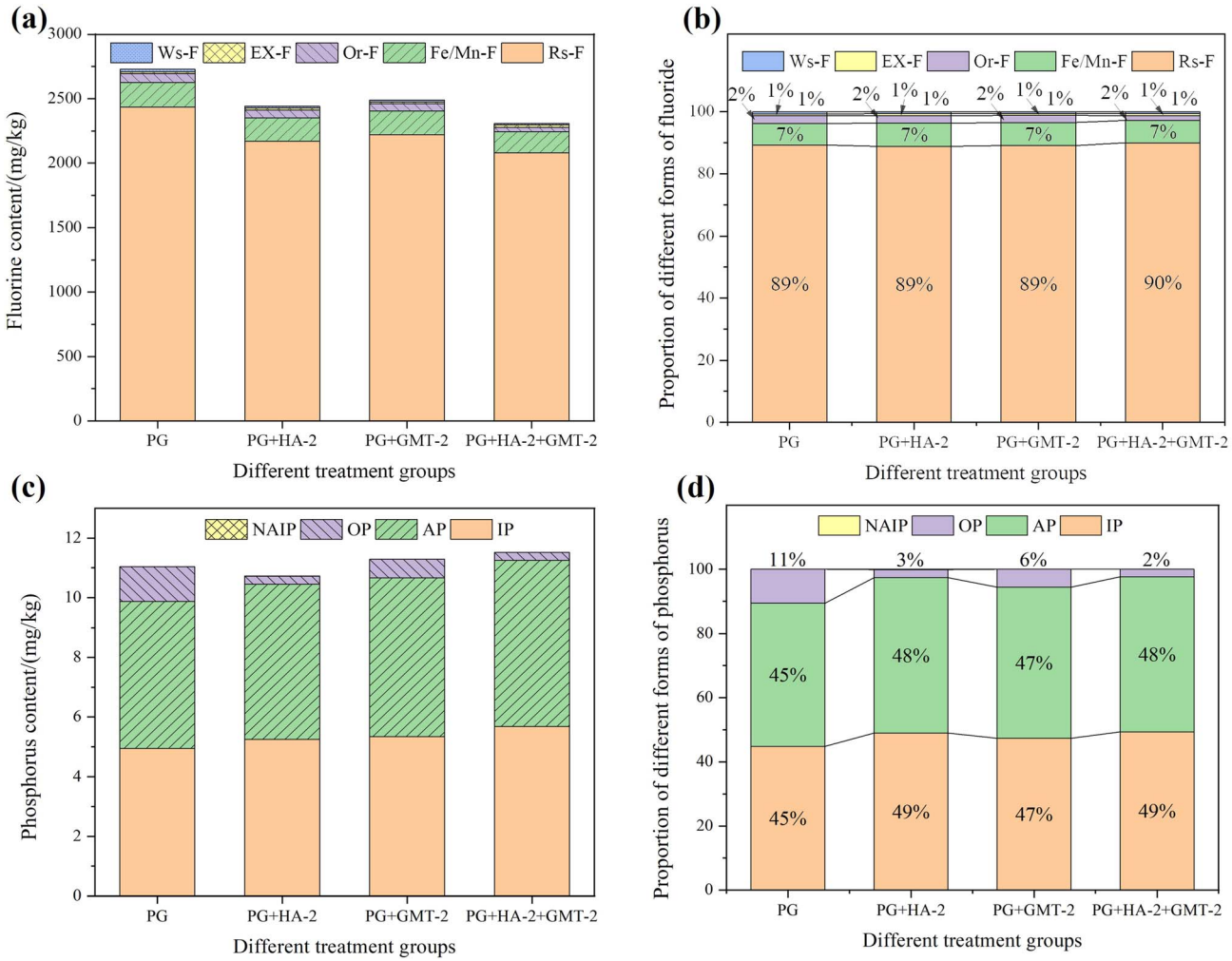

Fig. 6 Effects of HA-2, GMT-2 and HA-2 synergized with GMT-2 on the various forms of P and F in PG (a) content and (b) proportion of different forms of F. (c) content and (d) proportion of different forms of P.

hysteresis loops—characteristic of mesoporous materials. The sharp uptake at high relative pressures ($P/P_0 > 0.9$) indicates the presence of macropores or interparticle voids. The pore size distributions exhibit similar dominant ranges, confirming that the principal mesoporous characteristics of the material are preserved after treatment. This observation further confirms that the introduction of HA and GMT did not alter the inherent porous structure of the PG matrix, which is crucial for maintaining its structural stability during the curing and stabilization process. As shown in Fig. 7(c), the peak positions and intensity trends of the pore diameter width distribution curves of PG, PG + HA-2, PG + GMT-2, and PG + HA-2 + GMT-2 are almost identical, indicating that the pore diameter and pore volume distributions of the materials have been well preserved after modification. This structural stability is also consistent with the effective fixed phase observed in our previous research results (Fig. 6, 7(a) and (b)), suggesting that the enhanced curing property is attributed to the surface chemical interactions and the change in the P/F occurrence forms, rather than structural damage.

The broadening of the hysteresis loops, particularly evident for the PG and PG + HA-2 samples (green and red curves), visually demonstrates their more developed and intricate porous architectures. This superior pore network suggests that these materials could potentially outperform PG + GMT-2 in applications reliant on porous structure, such as adsorption, catalysis, or energy storage. The quantitative data in Fig. 7(c) reveal that PG + HA-2 and the composite PG + HA-2 + GMT-2 possess the most hierarchically porous structures. This is primarily attributed to the intercalation of bulky HA-2 molecules between the PG particles, which generates substantial new voids and provides abundant adsorption sites.[18] In contrast, combined with the XRD results, the amorphous cementitious products formed from the GMT-2 reactions tend to block pore channels, leading to a denser matrix. In the composite system (PG + HA-2 + GMT-2), while some porosity is filled, the structure achieves an optimal balance. The HA-2 establishes a porous framework with active sites, while the GMT-2-derived gels act as a 'reinforcing' agent. This synergy creates a composite that

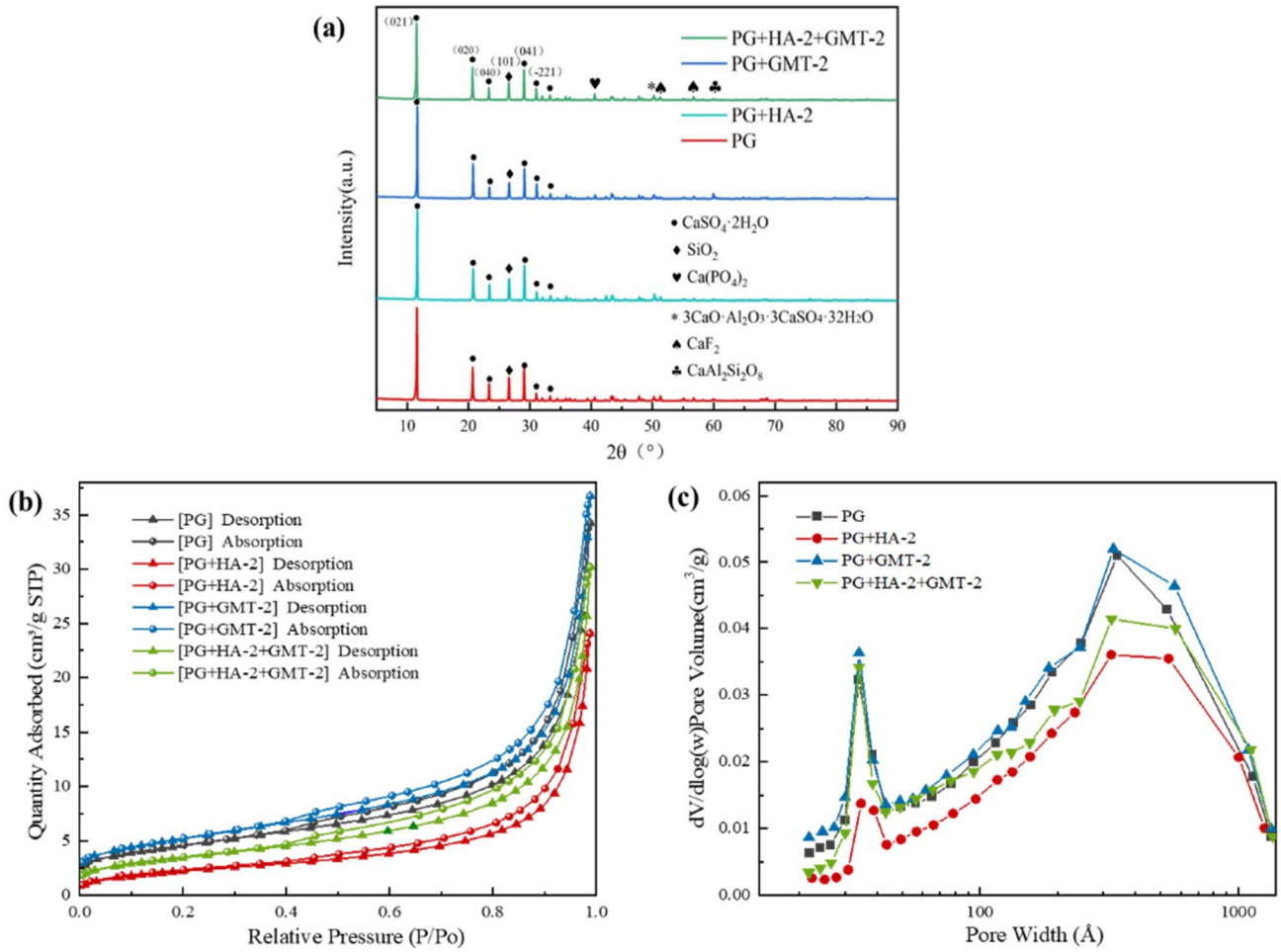

Fig. 7 (a) Influence of PG, HA-2, GMT-2 and HA-2 synergized with GMT-2 on the crystalline phases. (b) N_2 adsorption and desorption curves and (c) pore size distribution diagrams of PG.

retains beneficial porosity while achieving sufficient density to effectively sequester contaminants.

3.3.2 SEM characterization. Fig. 8 presents the SEM images of PG and the treated PG samples. In the treated PG samples (PG + HA-2, PG + GMT-2), irregular impurity particles, primarily originating from the P and F precipitates, are observed. The surfaces of the originally layered PG structures become progressively covered with these heterogeneous particles upon the addition of HA-2 or GMT-2. It can be observed that the HA particles are dispersed in PG, with a relatively clear interface, and there may be weak interactions. The GMT particles cover the PG, and a more obvious coating sensation is observed at the interface. Notably, the sample co-treated with HA-2 and GMT-2 (PG + HA-2 + GMT-2) displays a distinctly denser microstructure. The surface particles are more tightly interlocked, and the crystal surface morphology transitions from a smooth, dissolved appearance to an aggregated mass of angular, irregular particles, which might be a 'locking/bridging' structure formed on the surface. This transformation is attributed to the concurrent adsorption of HA and the metal-based amendment onto the PG surface, which facilitate the formation of stable compounds that encapsulate the flocculent impurities.[50] This encapsulation is a key mechanism for reducing the leaching potential of P and F.

3.3.3 FT-IR and XPS analysis. The FT-IR spectrum of raw PG displayed strong absorption bands at 3546.8 cm^{-1}, 3404.8 cm^{-1}, and 1621.4 cm^{-1}, indicating the presence of substantial crystalline water (Fig. 9). After treatment with HA-2, GMT-2, or their composite, the intensities of these bands were reduced, suggesting the loss of a part of the crystalline water during the process and further confirming its primary origin from the gypsum ($CaSO_4 \cdot 2H_2O$) structure. Concurrently, the intensity of the characteristic sulfate band at 1116.0 cm^{-1} also decreased in the treated samples, likely due to interactions between the additives and SO_4^{2-} ions, which altered their local chemical environment. The broad band at approximately 3400 cm^{-1} corresponded to the O–H and N–H stretching vibrations. Compared with pure PG and the binary composites, the ternary composite showed an obvious red shift and intensity attenuation in this region, suggesting enhanced hydrogen bonding and coordination interactions among PG, HA-2, and GMT-2. The band at 1686.7 cm^{-1} in PG was assigned to the

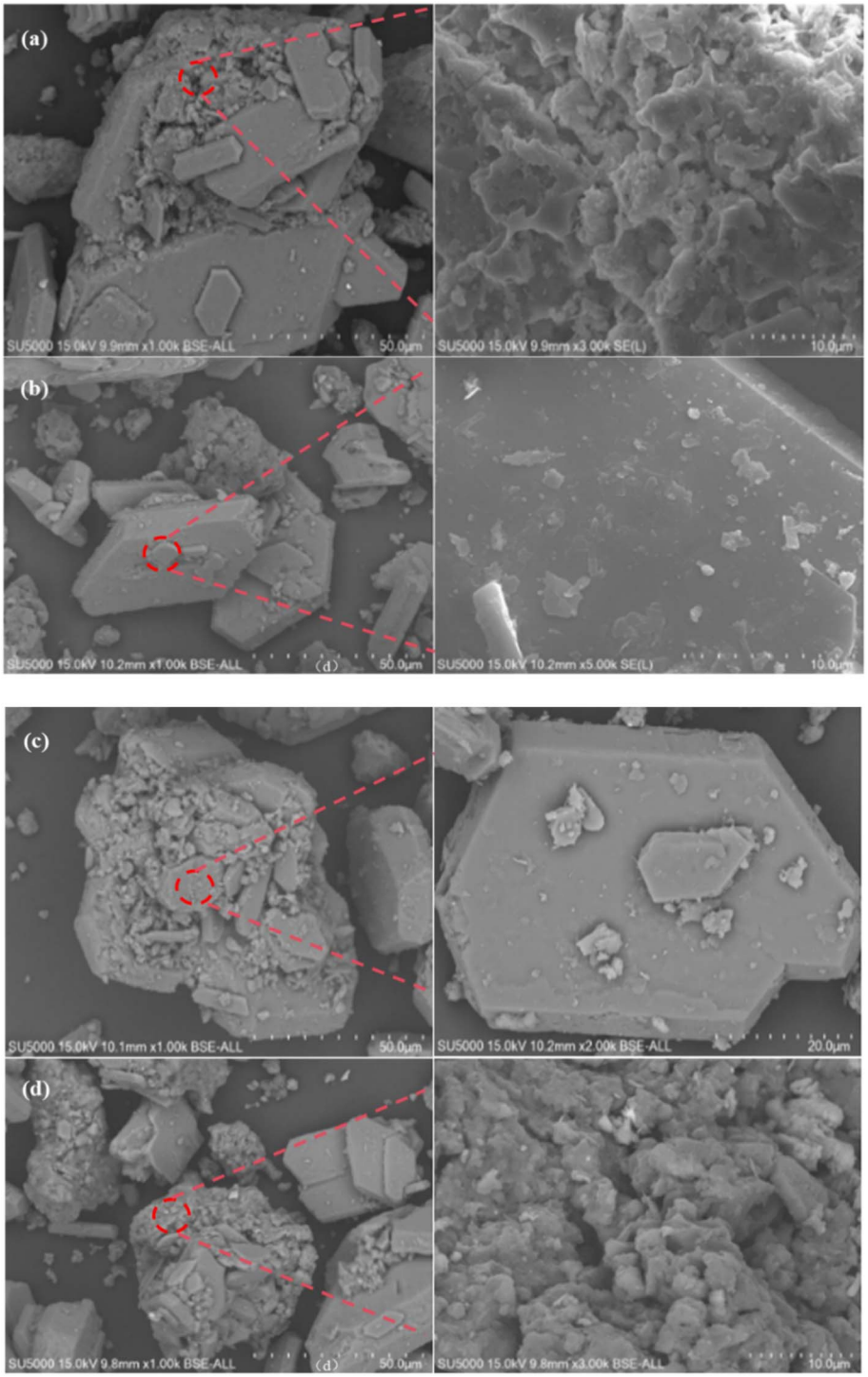

Fig. 8 SEM images of (a) PG, (b) PG + HA-2, (c) PG + GMT-2, and (d) PG + HA-2 + GMT-2 samples.

C═O stretching vibration, which shifted to 1621.4 cm^{-1} in the ternary system. The red shift in magnitude in the ternary composite was significantly larger than the sum of those in the two binary systems, demonstrating a non-additive synergistic effect. This result confirmed that carbonyl groups in PG served as molecular bridges to connect HA-2 and GMT-2 simultaneously.

The characteristic bands of PG at 2241.6 cm^{-1}, 797.9 cm^{-1}, and 669 cm^{-1} correspond to the vibrations of $H_2PO_4^-$, insoluble P, and PO_4^{3-}, respectively. A significant attenuation of these band intensities was observed in all the treated samples, demonstrating the effective immobilization of P in various forms. Treatment with HA-2 alone showed the most pronounced effect on P fixation. Notably, the composite sample

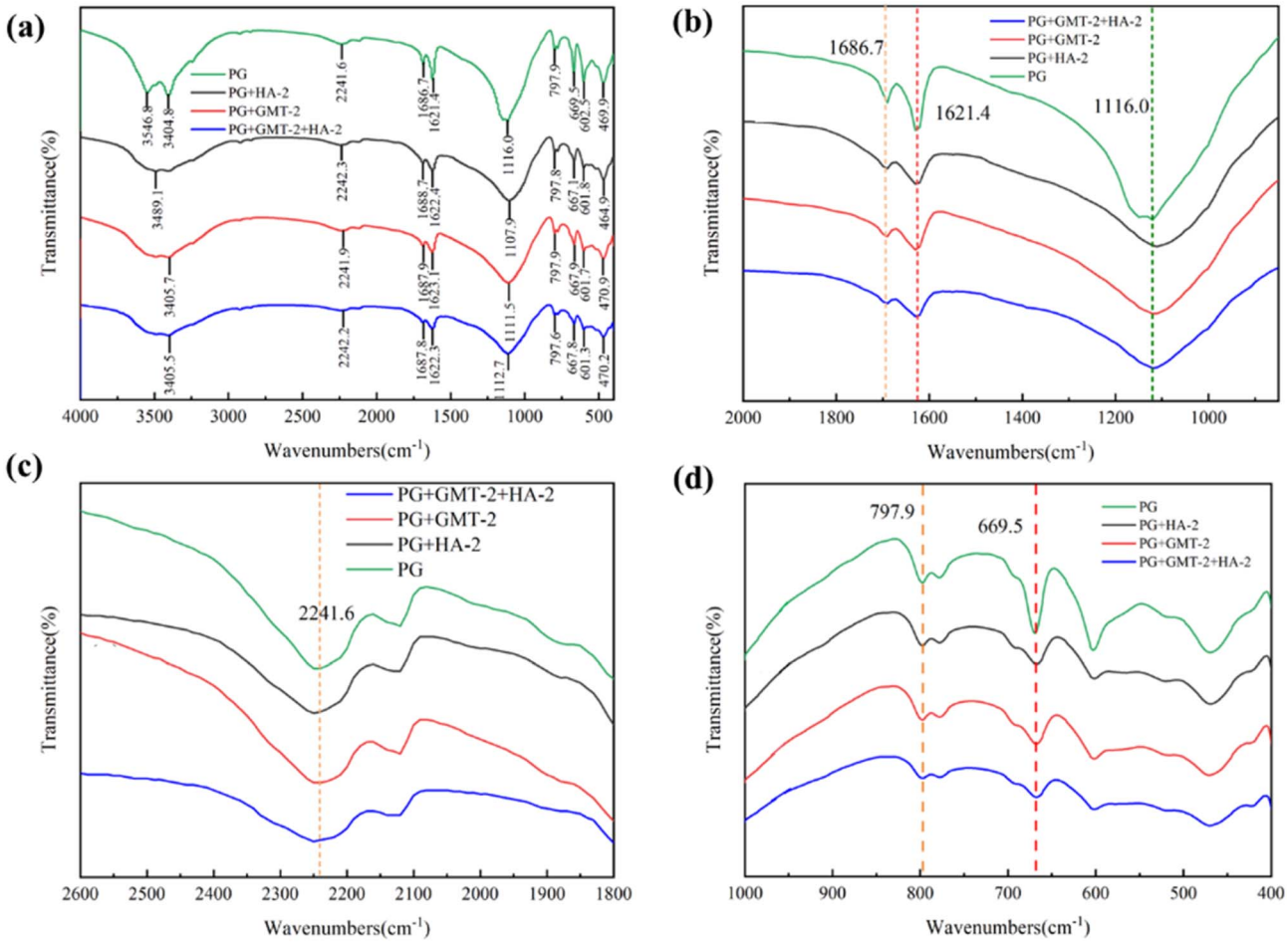

Fig. 9 FT-IR spectra of PG before and after solidification. The wavenumbers range from (a) 4000 cm^{-1} to 500 cm^{-1}, (b) 2000 cm^{-1} to 1000 cm^{-1}, (c) 2600 cm^{-1} to 1800 cm^{-1}, and (d) 1000 cm^{-1} to 400 cm^{-1}.

(PG + HA-2 + GMT-2) exhibited the greatest reduction in band intensity, revealing a synergistic enhancement in P immobilization when both additives were used. This finding is consistent with the P speciation analysis as discussed previously. Although the cementitious products formed are poorly crystalline or amorphous and thus do not produce distinct diffraction peaks, their presence was confirmed through complementary XRD and SEM analysis.

The XPS analysis provided pivotal evidence for the immobilization mechanism by revealing the changes in elemental concentrations and chemical environment on the surface. A significant increase in the atomic carbon (C) concentration was observed on the surface of all treated samples. For instance, in the PG + HA-2 sample, the C content increased from 60.55% to 74.17%, representing a rise of 22.5% (Table 3). Concurrently, the signals for calcium (Ca) and sulfur (S) were markedly attenuated. This provides direct evidence for the formation of an effective coating layer derived from HA and the amendment on the PG surface. The F 1s spectrum of raw PG (Fig. 10(a)) could be deconvoluted into three characteristic peaks with binding energies of 686.48 eV, 685.62 eV, and 684.67 eV, which are assigned to Na_2SiF_6, MgF_2, and NaF, respectively.[51] Notably, NaF and Na_2SiF_6 are soluble F salts and represent the major sources of mobile F responsible for the release risk associated with PG.

Table 3 Variations in the relative atomic concentrations of each element on the sample surface

	Relative atomic concentrations/%				
Samples	C	F	P	S	Ca
PG	60.55	2.56	3.10	15.29	18.50
PG + HA-2	74.17	1.22	2.16	11.14	11.30
PG + GMT-2	67.82	1.69	2.48	11.85	16.15
PG + HA-2 + GMT-2	73.00	1.17	2.06	11.97	11.80

Following treatment with HA-2, systematic changes were observed in the chemical environments of the P and F species on the PG surface, as shown in Fig. 10 and 11. The P 2p high-resolution spectrum revealed a systematic positive shift in the binding energies of the P species. The peaks corresponding to $H_2PO_4^-/HPO_4^{2-}$, $CaHPO_4 \cdot 2H_2O$, and $Ca_{10}(PO_4)_6F_2$ shifted by +0.10 eV, +0.18 eV, and +0.43 eV, respectively. This indicates a decreased electron cloud density around the P atoms, confirming that oxygen-containing functional groups from the HA engaged in complexation with the various P forms.

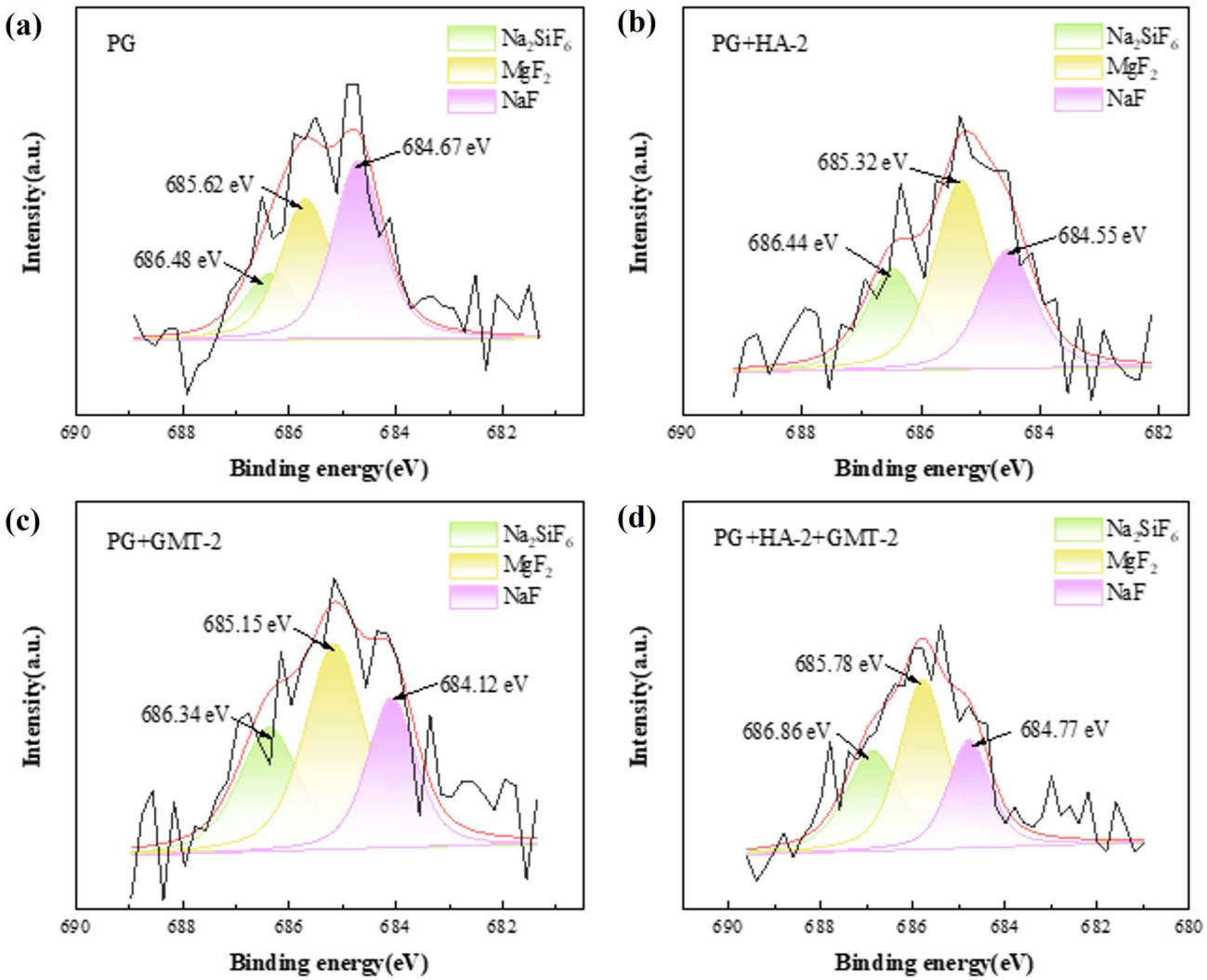

Fig. 10 High-resolution F 1s XPS spectra of (a) PG and before and after treatment with (b) PG + HA-2, (c) PG + GMT-2, and (d) PG + HA-2 + GMT-2.

Concurrently, in the F 1s spectrum, the binding energies for Na_2SiF_6, MgF_2, and NaF exhibited negative shifts of −0.04 eV, −0.30 eV, and −0.12 eV, respectively. This suggests an increased electron density around the F atoms, likely resulting from the partial conversion of soluble F into less soluble organo-F complexes *via* ion exchange with HA.

Treatment with GMT-2 also induced significant shifts in the binding energies of P and F species. In the P 2p spectrum, the peaks for $H_2PO_4^-/HPO_4^{2-}$, $CaHPO_4 \cdot 2H_2O$, and $Ca_{10}(PO_4)_6F_2$ shifted positively by +0.11 eV, +0.13 eV, and +0.24 eV, respectively. This indicates the involvement of GMT-2 in P fixation, likely through surface reactions or co-precipitation, forming new phases.[52] In the F 1s spectrum, the binding energies for Na_2SiF_6, MgF_2, and NaF shifted by −0.14 eV, −0.47 eV, and −0.55 eV, respectively. The substantial shift for NaF is consistent with the precipitation of sparingly soluble F (*e.g.*, MgF_2, CaF_2) by metal ions (Mg^{2+}, Ca^{2+}) released from GMT-2. The incorporation of F into a stable crystalline lattice increases the electron density around the F atom, resulting in a pronounced negative binding energy shift. The combined application of HA-2 and GMT-2 created a synergistic effect, integrating physical encapsulation with dual chemical fixation mechanisms – complexation and precipitation. The PG surface composition changed markedly, with the carbon content increasing by 20.5%, while calcium and sulfur decreased by 36.2% and 21.7%, respectively. This directly confirms the formation of an effective composite coating layer that masks the original gypsum surface.

In the PG + HA-2 + GMT-2 composite, the total P and F contents decreased by 33.5% and 54.3%, respectively. Notably, contrary to the individual treatments, all F species exhibited positive binding energy shifts (Na_2SiF_6 +0.38 eV, MgF_2 +0.16 eV, NaF +0.10 eV). If the combined effects were merely additive, the F 1s shift would be more negative. The reversal in shift direction strongly indicates the emergence of a novel chemical environment absent in single-component treatments. This suggests the formation of a ternary 'HA–F–metal ion' surface complex. In this structure, HA acts as a bridging ligand, with its functional

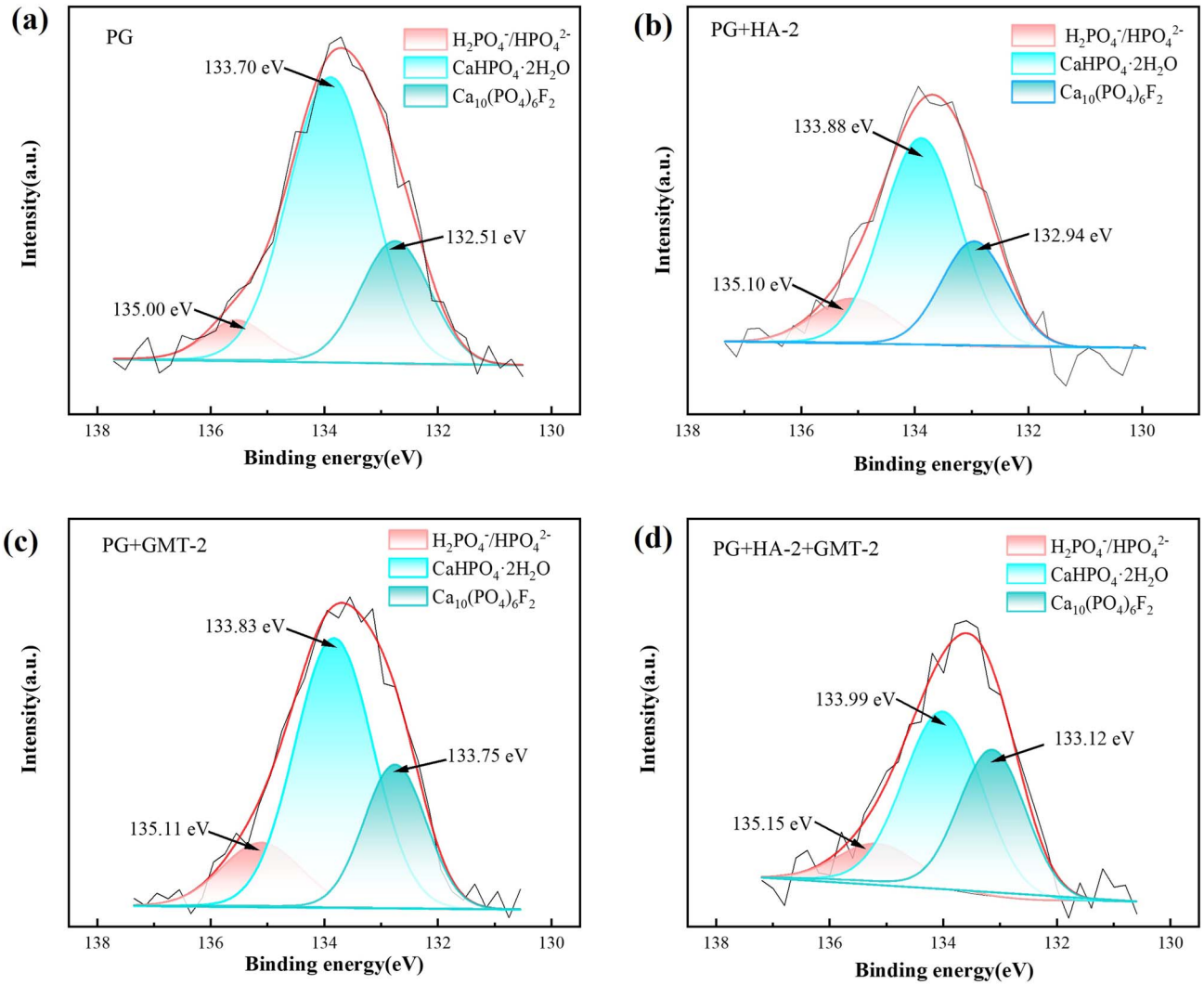

Fig. 11 High-resolution P 2p XPS spectra of (a) PG and before and after treatment with (b) PG + HA-2, (c) PG + GMT-2, and (d) PG + HA-2 + GMT-2.

groups simultaneously coordinating to the F species and metal ions (*e.g.*, Al^{3+}) supplied by GMT-2. This configuration creates a unique chemical environment around the F atom with reduced electron density. This highly stable 'bridging' fixation mechanism drastically inhibits F mobility, which is fully consistent with the observed lowest F leaching concentration in toxicity characteristic leaching procedure (TCLP) tests.

3.4 Mechanism of synergistic stabilization on P and F

The HA-2 and GMT-2 immobilize the P and F in PG through distinct primary mechanisms, and their combined application results in a significant synergistic enhancement (Fig. 12). The immobilization mechanism of HA-2 is predominantly based on surface complexation and coating. During physical coating, the bulky HA-2 molecules cannot penetrate the inner structure of PG and primarily adsorb onto the particle surfaces, forming an organic coating layer. This layer directly impedes the leaching of P and F, leading to the significant increase in the surface C content and the attenuation of Ca and S signals. Chemically, HA-2 fixes P mainly through the complexation reactions between its surface oxygen-containing functional groups (*e.g.*, carboxyl) and P ions, which reduces the electron cloud density around the phosphorus atoms (causing a positive shift in the P 2p binding energy) and anchors P onto the mineral surface. Its chemical fixation of F involves an ion exchange process, where H^+ from HA-2 replaces Na^+ in soluble F salts (*e.g.*, NaF and Na_2SiF_6), potentially forming sparingly soluble organo–fluorine complexes or adsorbing HF molecules, thereby increasing the electron density around F atoms (causing a negative shift in the F 1s binding energy). The immobilization mechanism of GMT-2 is centered on chemical precipitation and cementitious reactions. Chemical precipitation occurs *via* metal ions (*e.g.*, Ca^{2+}, Mg^{2+}, Fe^{3+}, and Al^{3+}) released from GMT-2, which react with soluble F in PG to form insoluble F precipitates (*e.g.*, CaF_2, MgF_2). Concurrently, these ions can also generate sparingly soluble microcrystalline P precipitates (*e.g.*, $Ca_3(PO_4)_2$). Furthermore, GMT-2 reacts with the PG components to form cementitious phases (*e.g.*, ettringite $3CaO \cdot Al_2O_3 \cdot 3CaSO_4 \cdot 32H_2O$ and $CaAl_2Si_2O_8$). These amorphous products promote interparticle flocculation and coagulation, creating a dense coating layer on the PG surface and within its pores that

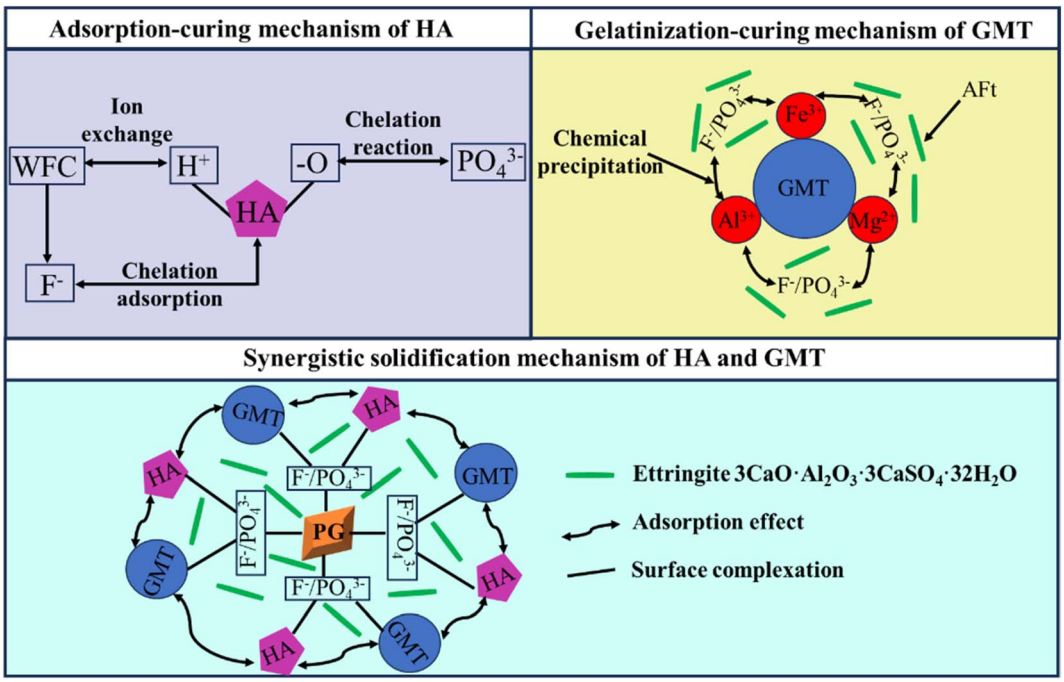

Fig. 12 Mechanism of the synergistic stabilization of P and F by HA and GMT.

encapsulates and immobilizes P and F. This process reduces the overall crystallinity of PG, as manifested by a decreased intensity and broadening of the XRD diffraction peaks.

The synergistic immobilization mechanism in the GMT-2 + HA-2 composite system primarily involves a bridge-enhanced effect combining physical coating and chemical fixation. The synergy is not a simple additive but achieves a '1 + 1 > 2' outcome. Both the immobilization efficiency (the greatest reduction in P and F content) and stability (the lowest F leaching concentration) surpass those of individual treatments. The core of this synergy lies in a 'bridging' fixation mechanism. HA-2 acts as a bridging molecule with its functional groups simultaneously binding to F species and coordinating with the metal ions (*e.g.*, Al^{3+}) supplied by GMT-2, forming a unique ternary 'HA–F–metal ion' surface complexation structure. This structure places the F atom in a new chemical environment with reduced electron density (resulting in a positive shift in the F 1s binding energy), which is extremely stable and greatly inhibits the release of F. SEM observations reveal a denser microstructure in the co-treated PG, with the surface particles tightly interlocked. This is attributed to the synergistic formation of a physical barrier comprising the HA-2 coating, GMT-2 cementitious products, and co-precipitated compounds, which collectively encapsulate PG crystals and effectively sequester P and F. In summary, HA-2 primarily immobilizes contaminants through surface adsorption and complexation, whereas GMT-2 functions mainly *via* precipitation and cementation. When applied together, the combined system leverages physical coating, chemical precipitation, and a distinctive bridged ternary complexation mechanism to construct a denser and more stable immobilization layer on the PG surface. This integrated approach results in the most effective and durable synergistic fixation of P and F achieved in this study.

4 Conclusions

This research demonstrates that a synergistic combination of 5 wt% HA-2 and 1 wt% GMT-2 effectively immobilizes P and F in PG. The treated material exhibits a leachate pH of 5.51 with the P and F concentrations as low as 0.1 mg L^{-1} and 0.9 mg L^{-1}, respectively, complying with China's class III surface water standards. The stabilization mechanism integrates physical coating, chemical precipitation, and a distinctive bridge-enhanced ternary complexation among HA, F, and metal ions from GMT, resulting in a denser and more stable fixation layer. This organic–inorganic approach offers a green, low-cost strategy for the environmentally sound management and resource utilization of PG.

Conflicts of interest

There are no conflicts to declare.

Data availability

The data are available from the corresponding author on reasonable request.

Supplementary information (SI) is available. See DOI: https://doi.org/10.1039/d6ra01271j.

Acknowledgements

This work was supported by the Yunnan Fundamental Research Projects (Grant No. 202501AU070112).

References

1 H. Li, J. Zhong, H. Zhang, C. Yin and Y. Cai, Effect of temperature on properties of II-anhydrite prepared by phosphogypsum with high-temperature fluidized calcination, *Process Saf. Environ. Prot.*, 2025, **198**, 107167.

2 H. Li, C. Yin, H. Zhang, J. Zhong and Y. Cai, Effect of water-soluble P2O5 and fluorine impurities on the properties of calcinated purified phosphogypsum, *Process Saf. Environ. Prot.*, 2025, **203**, 107969.

3 J. Shu, H. Wu, M. Chen, H. Peng, B. Li, R. Liu, Z. Liu, B. Wang, T. Huang and Z. Hu, Fractional removal of manganese and ammonia nitrogen from electrolytic metal manganese residue leachate using carbonate and struvite precipitation, *Water Res.*, 2019, **153**, 229–238.

4 H. Liu, L. Zhu, X. Tian and Y. Yin, Seasonal variation of bacterial community in biological aerated filter for ammonia removal in drinking water treatment, *Water Res.*, 2017, **123**, 668–677.

5 S.-Y. Oh and Y.-D. Seo, Distribution characteristics and analytical protocols for remediation of fluorine-contaminated soils at a phosphate-gypsum waste landfill, *Environ. Earth Sci.*, 2022, **82**(1), 26.

6 E. Bilal, H. Bellefqih, V. Bourgier, H. Mazouz, D.-G. Dumitraș, F. Bard, M. Laborde, J. P. Caspar, B. Guilhot, E.-L. Iatan, M. Bounakhla, M. A. Iancu, Ş. Marincea, M. Essakhraoui, B. Li, R. R. Diwa, J. D. Ramirez, Y. Chernysh, V. Chubur, H. Roubík, H. Schmidt, R. Beniazza, C. R. Cánovas, J. M. Nieto and N. Haneklaus, Phosphogypsum circular economy considerations: A critical review from more than 65 storage sites worldwide, *J. Cleaner Prod.*, 2023, **414**, 137561.

7 C. Wang, D. Xiong, Y. Chen, K. Wu, M. Tu, P. Wang, Z. Zhang and L. Zhou, Characteristic pollutant purification analysis of modified phosphogypsum comprehensive utilization, *Environ. Sci. Pollut. Res.*, 2022, **29**(44), 67456–67465.

8 S. Zhang, Y. Wang, L. Wang and J. Han, Research progress on comprehensive utilization of phosphogypsum and metallurgical acidic gypsum residue (*In Chinese*), *Chin. J. Eng.*, 2025, **47**(7), 1494–1514.

9 W. Zhang, L. Zhao, M. Xue, X. Duan, C. Feng and J. Zhu, Efficient precipitation of soluble phosphorus impurities in the recycling of phosphogypsum to produce hemihydrate gypsum, *J. Cleaner Prod.*, 2023, **396**, 136455.

10 M. Singh, M. Garg, C. L. Verma, S. K. Handa and R. Kumar, An improved process for the purification of phosphogypsum, *Constr. Build. Mater.*, 1996, **10**(8), 597–600.

11 J. Li, J. Chen, H. Huang, X. Chen, D. Xiao, S. Huang and Y. Li, Synergistic co-pyrolysis of phosphogypsum and sewage sludge for phosphorus recovery: a novel multi-pollutant control and resource utilization strategy, *Chem. Eng. J.*, 2025, **515**, 163846.

12 M. Salo, O. Knauf, J. Mäkinen, X. Yang and P. Koukkari, Integrated acid leaching and biological sulfate reduction of phosphogypsum for REE recovery, *Miner. Eng.*, 2020, **155**, 106408.

13 W. Shen, M. Zhou, W. Ma, J. Hu and Z. Cai, Investigation on the application of steel slag–fly ash–phosphogypsum solidified material as road base material, *J. Hazard. Mater.*, 2009, **164**(1), 99–104.

14 J. Shu, M. Chen, H. Wu, B. Li, B. Wang, B. Li, R. Liu and Z. Liu, An innovative method for synergistic stabilization/solidification of Mn^{2+}, NH_4^+-N, PO_4^{3-} and F^- in electrolytic manganese residue and phosphogypsum, *J. Hazard. Mater.*, 2019, **376**, 212–222.

15 J. Ren, J. Shao, M. Liu, H. Zhu, M. Li, R. Ma, L. Liang, J. Mao and D. Wang, The improvement on the properties and heavy metal solidification of phosphogypsum-steel slag cementitious material: Enhancement from Bi-directional carbonation, *Constr. Build. Mater.*, 2024, **457**, 139435.

16 Z. Sun, Y. Liao, Y. Zhang, S. Sun, Q. Kan, Z. Wu, L. Yu, Z. Dong, Z. Wang, R. He, L. Wang, Q. Meng, H. Wang, Q. Wang, L. Mao, D. Pan, S. Wang, Z. Zhang, W. Zhu, S. Liu, M. Wakeel, B. Hu, T. Duan, X. Tai and X. Wang, Sustainable carbon materials in environmental and energy applications, *Sustainable Carbon Mater.*, 2025, **1**(1), e007.

17 X. Pan, J. Ji, N. Zhang and M. Xing, Research progress of graphene-based nanomaterials for the environmental remediation, *Chin. Chem. Lett.*, 2020, **31**(6), 1462–1473.

18 D. Wang, Y. Tao, Y. Feng, D. Zhu, Q. Zhang and Q. Chen, Enhanced solidification/stabilization (S/S) of fluoride in smelting solid waste-based phosphogypsum cemented paste backfill utilizing biochar: Mechanisms and performance assessment, *J. Environ. Manage.*, 2024, **367**, 122088.

19 D. Nizevičienė, D. Vaičiukynienė, B. Michalik, M. Bonczyk, V. Vaitkevičius and V. Jusas, The treatment of phosphogypsum with zeolite to use it in binding material, *Constr. Build. Mater.*, 2018, **180**, 134–142.

20 C. Wenxiang, Y. Wei, P. Jiahui, L. Guogang and Y. Suhong, Preparation of anhydrite from phosphogypsum: Influence of phosphorus and fluorine impurities on the performances, *Constr. Build. Mater.*, 2022, **318**, 126021.

21 M. Pliaka and G. Gaidajis, Potential uses of phosphogypsum: A review, *J. Environ. Sci. Health, Part A*, 2022, **57**(9), 746–763.

22 H. Olvera-Vargas, J.-C. Rouch, C. Coetsier, M. Cretin and C. Causserand, Dynamic cross-flow electro-Fenton process coupled to anodic oxidation for wastewater treatment: Application to the degradation of acetaminophen, *Sep. Purif. Technol.*, 2018, **203**, 143–151.

23 M. P. Campos, L. J. P. Costa, M. B. Nisti and B. P. Mazzilli, Phosphogypsum recycling in the building materials industry: assessment of the radon exhalation rate, *J. Environ. Radioact.*, 2017, **172**, 232–236.

24 G. Jiang, L. Zhao, S. Wu, Y. Li, A. Wu, Y. He, H. Cheng, W. Sun and H. Li, A systematic review of cemented paste backfill technology for cleaner and efficient utilization of phosphogypsum in China, *Miner. Eng.*, 2025, **231**, 109468.

25 B. A. Gomes, F. L. Motta and M. H. A. Santana, Humic acids: Structural properties and multiple functionalities for novel technological developments, *Mater. Sci. Eng., C*, 2016, **62**, 967–974.

26 C. Huang, H. Zhang, W. Zeng, J. Ma, S. Zhao, Y. Jiang, C. Huang, H. Mao and Y. Liao, Enhanced fluoride adsorption of aluminum humate and its resistance on fluoride accumulation in tea leaves, *Environ. Technol.*, 2020, **41**(3), 329–338.

27 Y. Gao, A. Tariq, F. Zeng, J. Sardans, J. Peñuelas, Z. Zhang, W. Islam and M. Xu, "Fertile islands" beneath three desert vegetation on soil phosphorus fractions, enzymatic activities, and microbial biomass in the desert-oasis transition zone, *Catena*, 2022, **212**, 106090.

28 W. Huang, Y. Zhang and D. Li, Adsorptive removal of phosphate from water using mesoporous materials: A review, *J. Environ. Manage.*, 2017, **193**, 470–482.

29 B. Wu, J. Wan, Y. Zhang, B. Pan and I. M. C. Lo, Selective Phosphate Removal from Water and Wastewater using Sorption: Process Fundamentals and Removal Mechanisms, *Environ. Sci. Technol.*, 2020, **54**(1), 50–66.

30 Z. Zhao, M. Sun, J. Xia, H. Xu and Y. Wu, A specific calcium silicate hydrate (PC/SP/CA-H) for simultaneous removal of phosphate and fluoride from low concentration water: Feasible and mechanisms research, *J. Water Process Eng.*, 2025, **71**, 107312.

31 Y. Yang, A. Luo, C. Wu, J. Qu, X. Xiao, J. Wang, Y. Cao, P. Dong, R. Chi, Z. Xu and K. Zhang, Mechanochemical synthesis of Ca-Al-La layered double hydroxide for efficient soluble phosphorus immobilization in phosphogypsum, *Environ. Res.*, 2025, **285**, 122447.

32 J. Zhang, H. Tan, X. He, W. Yang and X. Deng, Utilization of carbide slag-granulated blast furnace slag system by wet grinding as low carbon cementitious materials, *Constr. Build. Mater.*, 2020, **249**, 118763.

33 M. Klučáková, Dissociation properties and behavior of active humic fractions dissolved in aqueous systems, *React. Funct. Polym.*, 2016, **109**, 9–14.

34 T. Lan, P. Wu, Z. Liu, M. Stroet, J. Liao, Z. Chai, A. E. Mark, N. Liu and D. Wang, Understanding the Effect of pH on the Solubility and Aggregation Extent of Humic Acid in Solution by Combining Simulation and the Experiment, *Environ. Sci. Technol.*, 2022, **56**(2), 917–927.

35 D. Cardoso, A. Narcy, S. Durosoy, C. Bordes and Y. Chevalier, Dissolution kinetics of zinc oxide and its relationship with physicochemical characteristics, *Powder Technol.*, 2021, **378**, 746–759.

36 X. Chen, Q. Wang, Q. Wu, X. Xie, S. Tang, G. Yang, L. Luo and H. Yuan, Hydration reaction and microstructural characteristics of hemihydrate phosphogypsum with variable pH, *Constr. Build. Mater.*, 2022, **316**, 125891.

37 L. Chen, T. Zhou, J. Yang, J. Qi, L. Zhang, T. Liu, S. Dai, Y. Zhao, Q. Huang, Z. Liu and B. Li, A review on the roles of biochar incorporated into cementitious materials: Mechanisms, application and perspectives, *Constr. Build. Mater.*, 2023, **409**, 134204.

38 Z. Zhou, Y. Lu, W. Zhan, L. Guo, Y. Du, T. C. Zhang and D. Du, Four stage precipitation for efficient recovery of N, P, and F elements from leachate of waste phosphogypsum, *Miner. Eng.*, 2022, **178**, 107420.

39 Z. Li, Chemical forms of fluorine in soils from 12 tea gardens of Fenghuang mountain, east of Guangdong Province (*in Chinese*), *Environ. Chem.*, 2011, **30**(6), 1193–1198.

40 E. J. Reardon and Y. Wang, A Limestone Reactor for Fluoride Removal from Wastewaters, *Environ. Sci. Technol.*, 2000, **34**(15), 3247–3253.

41 B. Li, J. Shu, L. yang, C. Tao, M. Chen, Z. Liu and R. Liu, An innovative method for simultaneous stabilization/solidification of PO43− and F− from phosphogypsum using phosphorus ore flotation tailings, *J. Cleaner Prod.*, 2019, **235**, 308–316.

42 H. Wang, Z. Yang, X. Li and Y. Liu, Distribution and transformation behaviors of heavy metals and phosphorus during hydrothermal carbonization of sewage sludge, *Environ. Sci. Pollut. Res.*, 2020, **27**(14), 17109–17122.

43 C. Lin, S. Li, B. Zhu, S. Liu, F. Li, Z. Zhou and T. Li, Al-PHOSLOCK thin-layer capping to control phosphorus release from sediment: effect of hydraulic retention time and phosphorus migration/transformation mechanism, *J. Soils Sediments*, 2021, **21**(6), 2474–2482.

44 X. Lv and L. Xiang, The Generation Process, Impurity Removal and High-Value Utilization of Phosphogypsum Material, *Nanomaterials*, 2022, 3021.

45 J. Zhou, L. Yang, Q. Lin and J. X. Cao, Analysis of Phosphogypsum's Physical and Chemical Properties and Making of Anhydrite Cement from Phosphogypsum, *Appl. Mech. Mater.*, 2013, **275–277**, 2131–2135.

46 M. I. Romero-Hermida, A. M. Borrero-López, F. J. Alejandre, V. Flores-Alés, A. Santos, J. M. Franco and L. Esquivias, Phosphogypsum waste lime as a promising substitute of commercial limes: A rheological approach, *Cem. Concr. Compos.*, 2019, **95**, 205–216.

47 Y. Wang, L. Yu, H. Yuan, D. Ying and N. Zhu, Improved removal of phosphorus from incinerated sewage sludge ash by thermo-chemical reduction method with CaCl2 application, *J. Cleaner Prod.*, 2020, **258**, 120779.

48 B. El-Eswed and F. Khalili, Adsorption of Cu(II) and Ni(II) on solid humic acid from the Azraq area, Jordan, *J. Colloid Interface Sci.*, 2006, **299**(2), 497–503.

49 Y. Li, Q. Yue and B. Gao, Adsorption kinetics and desorption of Cu(II) and Zn(II) from aqueous solution onto humic acid, *J. Hazard. Mater.*, 2010, **178**(1), 455–461.

50 B. Xing, M. Ouyang, N. Graham and W. Yu, Enhancement of phosphate adsorption during mineral transformation of natural siderite induced by humic acid: Mechanism and application, *Chem. Eng. J.*, 2020, **393**, 124730.

51 M. Zhang, Y. Mei, Y. Li and J. Xia, Research on the technology and mechanism of direct acidification of phosphogypsum and deeply solidify impurities with lime, *J. Environ. Chem. Eng.*, 2024, **12**(6), 114937.

52 X. Chen, X. Tan, Y. Yu, H. Ye and S. Chen, From hazardous waste to backfill materials: deep stabilization of soluble fluoro-phosphorus in phosphogypsum flotation tailings via mechanochemical-geopolymer coupling technology, *Chem. Eng. J.*, 2025, **522**, 167975.